ACS APPLIED MATERIALS & INTERFACES

www.acsami.org

Research Article

Electrocatalyst Derived from Waste Cu−Sn Bronze for CO_2 Conversion into CO

Sasho Stojkovikj, Gumaa A. El-Nagar,* Frederik Firschke, Laura C. Pardo Pérez, Léo Choubrac, Metodija Najdoski, and Matthew T. Mayer*

Cite This: *ACS Appl. Mater. Interfaces* 2021, 13, 38161−38169

Read Online

ACCESS | Metrics & More | Article Recommendations | Supporting Information

ABSTRACT: To sustainably exist within planetary boundaries, we must greatly curtail our extraction of fuels and materials from the Earth. This requires new technologies based on reuse and repurposing of material already available. Electrochemical conversion of CO_2 into valuable chemicals and fuels is a promising alternative to deriving them from fossil fuels. But most metals used for electrocatalysis are either endangered or at serious risk of limitation to their future supply. Here, we demonstrate a combined strategy for repurposing of a waste industrial Cu−Sn bronze as a catalyst material precursor and its application toward CO_2 reuse. By a simple electrochemical transfer method, waste bronzes with composition $Cu_{14}Sn$ were anodically dissolved and cathodically redeposited under dynamic hydrogen bubble template conditions to yield mesoporous foams with $Cu_{10}Sn$ surface composition. The bimetal foam electrodes exhibited high CO_2 electroreduction selectivity toward CO, achieving greater than 85% faradaic efficiency accompanied by a considerable suppression of the competing H_2 evolution reaction. The Cu−Sn foam electrodes showed good durability over several hours of continuous electrolysis without any significant change in the composition, morphology, and selectivity for CO as a target product.

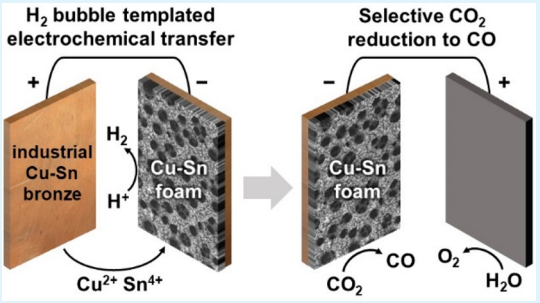

KEYWORDS: *electrochemical CO_2 conversion, Cu−Sn bronze, Cu−Sn foam, waste repurposing, carbon monoxide synthesis, electrodeposition, electrocatalysis*

INTRODUCTION

To develop a sustainable global society, it is crucial that we adapt our material consumption habits to fall within planetary boundaries. This will require limiting the extraction of materials from the Earth and developing alternative strategies based on repurposing and recycling the materials already available. Central to this effort is to slow the use of fossil-based sources of carbon to avoid unbalanced CO_2 emissions, which are contributing to climate change.[1] A sustainable alternative is to utilize CO_2 itself as a carbon feedstock, thereby transforming a waste product into a resource. Electrochemical reduction is an attractive method for CO_2 valorization under mild conditions driven simply by electricity.[2] While there are numerous possible products of CO_2 electrochemical reduction (CO_2ER),[3] carbon monoxide (CO) is currently one of the most techno-economically viable.[4] It is an important industrial feedstock that can be further converted into other valuable compounds using well-established technologies (e.g., the Fischer−Tropsch process).[5] Implementing CO_2ER (using renewable electricity and captured CO_2) to displace conventional routes of CO production could have a significant impact on decreasing CO_2 emissions.

We must keep in mind that a massive global transition to clean energy technologies will require massive quantities of raw materials, namely, metals, for building the new energy systems.[6] Because scalability is a prerequisite for these technologies, we will need to largely avoid materials of low abundance or availability. For CO_2ER this presents particular challenges for catalyst design. Although the best-known catalysts for electrochemical CO production are the precious metals Ag and Au,[7−9] recent studies have discovered a number of new catalysts for this reaction that are based on more abundant elements.[10] For instance, bimetallic combinations of Cu and Sn have demonstrated high activity and selectivity for CO_2 reduction to CO.[11−23] Although Cu and Sn are certainly more abundant than Ag and Au, both Cu and Sn are considered potentially endangered elements with increasingly limited availability and risk to their future supply.[6,24,25] With the goal of sustainable development, it is important that we look to existing raw or recycled materials, rather than new extractions, to supply new green technologies that must be implemented on a massive scale. Considering sources of Cu and Sn, a major application of both is their use in Cu−Sn

Received: March 17, 2021
Accepted: June 21, 2021
Published: August 9, 2021

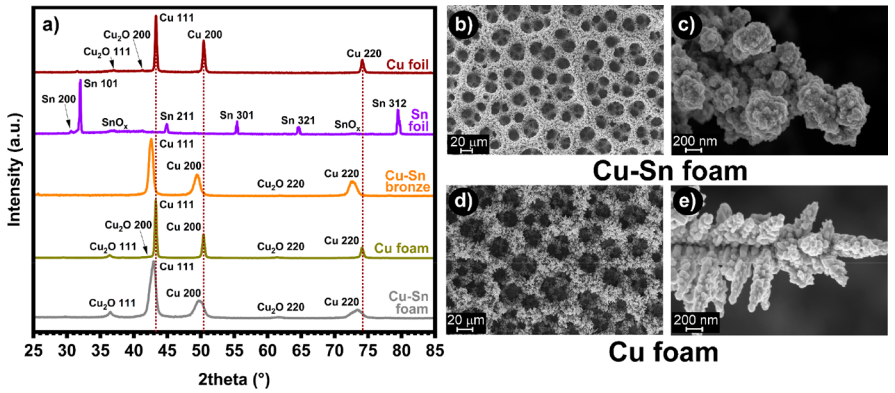

Figure 1. (a) Measured GI-XRD patterns of Cu foil (corresponds to JCPDS No. 04-0836), Sn foil (corresponds to JCPDS No. 01-086-2264), Cu−Sn bronze (corresponds to JCPDS No. 44-1477), Cu foam, and as-prepared Cu−Sn foam. SEM images of porous foams composed of dendrite-like microstructures: (b, c) Cu−Sn foam and (d, e) pure Cu foam.

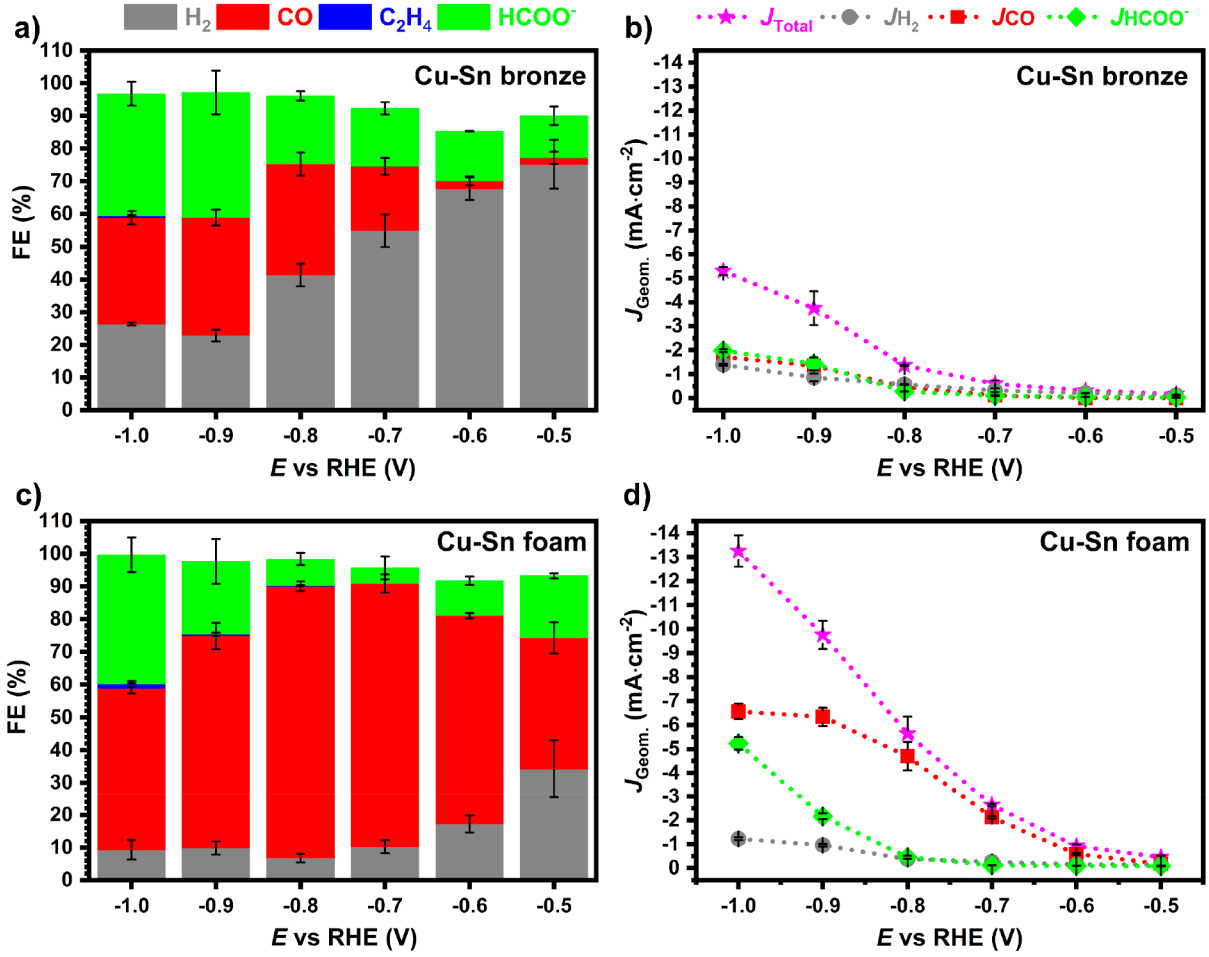

Figure 2. Electrocatalytic activity results; distribution of FEs and partial current densities for detected products at various potentials: (a) FEs and (b) total and partial current densities for products obtained on pristine Cu−Sn bronze; (c) FEs and (d) total and partial current densities obtained on Cu−Sn foam. All results are expressed as average values ± average mean absolute errors from replicate samples.

bronzes, attractive for their physical properties and use across a wide range of applications. Although the term "bronze" can refer to a wide range of alloys based on combining copper with other metals or metalloids in a variety of combinations and amounts, herein we refer to bronze only based on Sn as the major secondary element, a modern composition that is widely used in monuments, streetlamps, chandeliers, cutlery, and mechanical components including screws, nuts, washers, bearings, and gears.[26] These machine elements have a limited lifetime and need to be replaced, thus generating waste. Noting that one of the most common Cu−Sn bronzes has a Sn content (9−13 wt %) comparable to some recently reported Cu−Sn CO_2ER electrocatalysts,[17,19,20] we hypothesized that waste Cu−Sn bronzes could be repurposed for this application,

https://doi.org/10.1021/acsami.1c05015
ACS Appl. Mater. Interfaces 2021, 13, 38161−38169

either directly or with some modifications. An example is the utilization of leaded bronze, commonly used for production of bearings, for CO_2 to $HCOO^-$ conversion.[27]

This study introduces a simple, controllable, and potentially inexpensive strategy to repurpose industrial waste Cu−Sn bronze by employing it as a starting material for fabrication of electrocatalyst materials with a good selectivity for electroreduction of CO_2 into CO. By our method, industrial waste Cu−Sn bronze is converted into CO-selective electrocatalyst materials via a simple electrochemical transfer strategy, where Cu−Sn foams with high electrochemically active surface areas and controlled Cu−Sn composition were created from the planar waste Cu−Sn bronze.

RESULTS AND DISCUSSION

Samples of Cu−Sn bronze were obtained from the smelting facility RŽ Institut AD, Skopje, where they were prepared from molten Cu−Sn bronze wastes and cast into ingots (Figure S1, Supporting Information). These were cut into smaller rectangular platelike samples and mechanically polished prior to the characterization to eliminate any effect from surface inhomogeneities and to attain a near-planar surface (Figure S2). The detailed description of the applied pretreatments on the obtained waste Cu−Sn bronze is described in section S1.2. of the Supporting Information (SI).

The in-depth bulk, spatial, and surface characterization of the waste Cu−Sn bronze is of great importance for this research because it is utilized as a precursor for CO_2ER electrocatalyst preparation. Thus, the bulk and surface compositions of the waste Cu−Sn bronze were first investigated by ICP-OES, XRF, and EDX, as described in section S1.3 of the SI. This material showed a nominal bulk chemical composition of $Cu_{14}Sn$ (Table S1) on the basis of its ICP-OES analysis. The obtained XRF (Figure S3 and Table S2) and EDX (Figure S4) results show the distribution of both Cu and Sn with a nominal chemical composition of Cu_xSn with x = 14−16, which is in a good agreement with the ICP-OES results (Tables S1 and S2 and Figures S3 and S4). The GI-XRD characterization of the Cu−Sn bronze (Figure 1a) shows the typical diffraction peaks of Cu-rich α-bronze, in agreement with the reported results for similar materials with comparable Cu−Sn compositions.[17,20] The reflection peaks of the Cu−Sn bronze are broader and shift to smaller angles in comparison with the polycrystalline Cu foil ones. This can be attributed to the slightly larger lattice parameters in the crystal structure,[17] suggesting different structural identity in comparison to pristine Cu and Sn. That is, the presence of Sn in the alloy's crystal structure is affecting the position and width of the Cu diffraction peaks, but Sn itself does not show any noticeable signal. The surface composition of the Cu−Sn bronze was further investigated by XPS, which shows peaks only for elements Cu, Sn, and O (Figure S5). The surface Cu/Sn ratio of the Cu−Sn bronze is estimated from XPS to resemble $Cu_{14}Sn$ stoichiometry (in Table S3), which is in a good agreement with its bulk composition as estimated from XRF, ICP-OES, and EDX.

As the waste Cu−Sn bronze composition resembles that of some CO_2 reduction catalysts known for achieving good selectivity for CO production,[17,19,20] we first studied a bare Cu−Sn bronze directly as a CO_2 electrocatalyst to examine its intrinsic activity. The sample was connected to a wire and masked in PTFE tape to define a fixed active area and was tested in a three-electrode configuration in aqueous 0.1 mol·dm^{-3} $KHCO_3$ with bubbled CO_2 saturating the solution (Scheme S2). The electrodes were tested under potentiostatic control at several potentials, and generated gas and liquid products were analyzed by chromatography. See section S1.5 for a detailed explanation of the electrocatalysis activity testing. As shown in Figure 2a, the Cu−Sn bronze could reduce CO_2 to both $HCOO^-$ and CO at comparable faradaic efficiencies, while simultaneously producing significant amounts of H_2 at most applied potentials. For practical applications, a mixture of multiple products is usually undesirable, and chemical separation processes are challenging and expensive,[28] and thus designing CO_2ER catalysts that are selective for a single desired product is a central challenge in the field. This Cu−Sn bronze is therefore an inadequate CO_2ER electrocatalyst in its current form, so we next sought to use it as a precursor for synthesis of more complex nanostructured and selective electrocatalyst materials with a controlled Cu/Sn surface ratio and higher roughness and active site density.

Our goal was to take advantage of the near-ideal Cu−Sn composition of the Cu−Sn bronze and use it as starting material to create electrodes with tunable nanostructure morphologies because it has previously been shown that the electrode morphology can play a significant role in influencing product selectivity.[29,30] We explored a variety of different chemical and electrochemical methods for tuning the morphology and composition of the waste Cu−Sn bronze by dissolution and redeposition (see section S3 for a discussion of the strategies). We devised a simple strategy to electrochemically transfer the material from one substrate to another, via anodic dissolution, transport through the solution, and cathodic redeposition. As summarized in Scheme 1, the synthesis was conducted by arranging two cleaned Cu−Sn bronze samples as the anode and cathode in a solution of 1.5 mol·dm^{-3} H_2SO_4(aq) and applying a constant potential of −2.9 V vs Ag/AgCl to the cathode working electrode for a fixed duration. See section S1.4 and Figure S7 for a detailed

Scheme 1. Potentiostatically Controlled Dynamic H_2 Bubbling Templated (DHBT) Co-electrodeposition of Cu−Sn Porous Foam with a Surface Composition of $Cu_{10}Sn$ via Utilization of Cu−Sn Bronze as the Anode with a Surface Composition of $Cu_{14}Sn$[a]

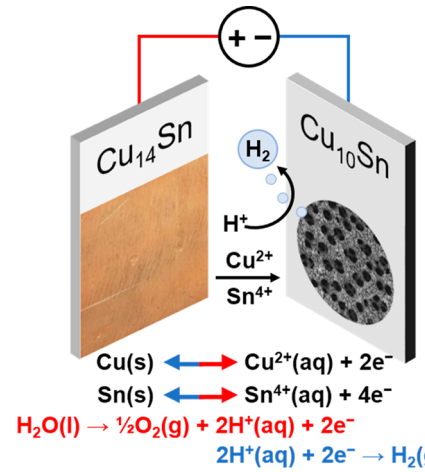

[a]Anode and cathode processes are shown in red and blue, respectively. A cathode potential of −2.9 V vs Ag/AgCl is applied (reference electrode not depicted).

https://doi.org/10.1021/acsami.1c05015
ACS Appl. Mater. Interfaces 2021, 13, 38161−38169

description of the method. Under these conditions, oxidation and reduction of the metals of the Cu−Sn bronze occur at the anode and cathode, respectively. At the cathode, the simultaneous reductive deposition of metals and H_2 evolution (from H^+ reduction) is used as a strategy to influence the nano- and mesoscale morphology of the deposited material via the so-called dynamic H_2 bubbling template (DHBT) phenomenon.[31]

The electrochemical transfer of Cu and Sn under DHBT conditions resulted in porous foamlike microstructures, as shown in Figure 1b,c and Figure S8. The in situ generated H_2 bubbles resulted in a deposited porous material with an interconnected structure around pores with an average pore diameter of 24 μm. At higher magnification (Figure 1c), it is seen that the pore walls form a nanoscale morphology of textured particles with a dendrite-like structure. Pure Cu foam was prepared using the same strategy for the purpose of comparison and to help in distinguishing the influences of roughness and composition on the Cu−Sn foams selectivity. Although both the pure Cu (Figure 1d,e) and Cu−Sn foams showed highly porous dendrite microstructures, their respective pore size, thickness, and nanoscale dendrites are quite different, as seen in Figure 1c,e, Figures S8−S10, and Table S4. The pure Cu foam is thicker (~82 μm) with slightly larger average pore sizes (~32 μm) and dendrites resembling a fern plantlike structure with sharp edges, whereas the Cu−Sn foam is thinner (~38 μm) with a smaller pore size (~24 μm) composed of blunted edge dendrites building from aggregated Cu−Sn bimetallic particles. To assess the electrochemically active surface area, we measured and used the double-layer capacitance (C_{DL}) of the samples to estimate the relative roughness factor of the foams versus their planar counterparts (see section S1.5). The Cu−Sn foam showed a significant increase of about 16-fold compared to the bare bronze, as well as a 2-fold higher roughness than that of the reference Cu foam prepared by the same technique, despite the fact that its total thickness was about half that of the Cu foam counterpart (Figure S12 and Table S6). The higher roughness of the Cu−Sn foam can be attributed to the differences in dendrite morphology and arrangement, together with its smaller average pore size compared to the reference pure Cu foam (Table S5).

The as-prepared Cu−Sn foam from the waste Cu−Sn bronze exhibited diffraction peaks of Cu(111), Cu(200), and Cu(220) planes like that of the pristine waste bronze, as shown in Figure 1a. These peaks are broader and slightly shifted toward lower angles compared to those of Cu foil and the pure Cu foam prepared via the same DHBT synthesis method (see section S1.4). This could be attributed to its smaller crystallites and/or the strain effect due to the chemical composition changes. Moreover, both Cu−Sn and Cu foams showed additional reflection peaks (Figure 1a) attributed to Cu_2O oxide coming from surface oxidation under air exposure, which are more noticeable than in the case of the near-planar Cu foil and Cu−Sn bronze. This is expected because the higher surface area of the pure Cu and Cu−Sn foams makes them prone to oxidation.

After establishing this method for synthesizing porous and rough Cu−Sn foams from the planar waste Cu−Sn bronze, we examined their bulk and surface compositions to evaluate whether they retained the composition of the starting material. The elemental mapping EDX analysis of the Cu−Sn foam suggests a homogeneous distribution of Cu and Sn over the entire Cu−Sn foam, as shown in Figure S11. Precise surface composition of the foams was determined by XPS (Figures S5 and S6 and Table S3). The Cu−Sn foam created from the waste bronze showed a surface composition of $Cu_{10}Sn$, which differed somewhat from the original composition of the pristine bronze Cu_xSn, x = 14−16 (as discussed in more detail below). In contrast, the EDX results show that the Sn bulk abundance is much lower than that in the pristine Cu−Sn bronze (Table S3).

The electrocatalytic activity results for the pristine Cu−Sn bronze are presented in Figure 2a,b and Figure S16. As discussed above, the CO_2 electroreduction performance of the pristine Cu−Sn bronze is poor in terms of selectivity, dominated by the thermodynamically favorable HER instead of CO_2ER at potentials more positive than −0.8 V vs RHE (all potentials hereafter are relative to RHE unless otherwise stated). Negative of −0.8 V, it generates CO and $HCOO^-$ with a comparable selectivity (~35−40%) while HER diminishes. The poor CO_2ER selectivity of the pristine bronze could be mainly attributed to its low electrochemically active surface area.[32,33]

The Cu−Sn foam showed quite different CO_2 electrocatalytic behavior in comparison with the pristine Cu−Sn bronze (Figure 2a,c and Figure S13a,b), most notable in its strong suppression of the HER at all applied potentials and emergence of CO as a dominant product. The bare Cu−Sn bronze and Cu−Sn foam showed comparable Tafel slopes, suggesting similar kinetics for the rate-determining step, as shown in Figure S14. The estimated Tafel slope values for the synthesized materials are in good agreement with the reported Tafel slopes for similar materials including Cu−Sn foam[19] and 3D hierarchical Cu−Sn structures and Cu−Sn rods.[23] The Cu−Sn foam exhibits FE of ~90% for C1 products (CO + $HCOO^-$) in the range between −0.7 and −1.0 V (Figure 2c and Figure S13b). Similarly, as in the case of the pristine Cu−Sn bronze, the FE for H_2 decreases when applying more negative potentials, although not changing much in the potential window from −0.8 to −1.0 V. Surprisingly, both the pristine bronze and Cu−Sn foam exhibited comparable Tafel slopes for HER with almost the same kinetics, as shown in Figure S14. Contrary to that of the HER, the FE for CO increases at more negative potentials, reaching a maximum of >85% at −0.8 V. This corresponds with a climbing CO partial current density toward a plateau at around −6 $mA{\cdot}cm^{-2}$ (Figure 2d). Whereas the CO generation appears limited to this rate at higher potentials, the rate of the $HCOO^-$ formation steeply increases at −0.9 V and beyond. Indeed, the enhanced CO production on Cu−Sn foam is believed to originate from the significantly slower $HCOO^-$ production kinetics, as demonstrated by the higher Tafel slope of $HCOO^-$ production on Cu−Sn foam compared to that of the pristine bronze.

The simultaneous discussion of both faradaic efficiency and partial current density is necessary to see the full picture toward understanding the electrocatalytic behavior of the prepared Cu−Sn foam because observing only the FE can be misleading. For instance, whereas the FE for CO decreases with a further increase of the cathodic potential beyond −0.8 V, its production rate does not decrease, as revealed from its steady-state partial current density. This suggests that CO_2ER into CO may be mass-transport-limited at higher negative potentials. The Cu−Sn foam showed ~2.5-fold higher FE for CO at −0.8 V with a 10-fold higher CO partial current density than the pristine Cu−Sn bronze at the same potential (Figure 2b,d). The observed enhanced CO_2ER on Cu−Sn foam could

https://doi.org/10.1021/acsami.1c05015
ACS Appl. Mater. Interfaces 2021, 13, 38161−38169

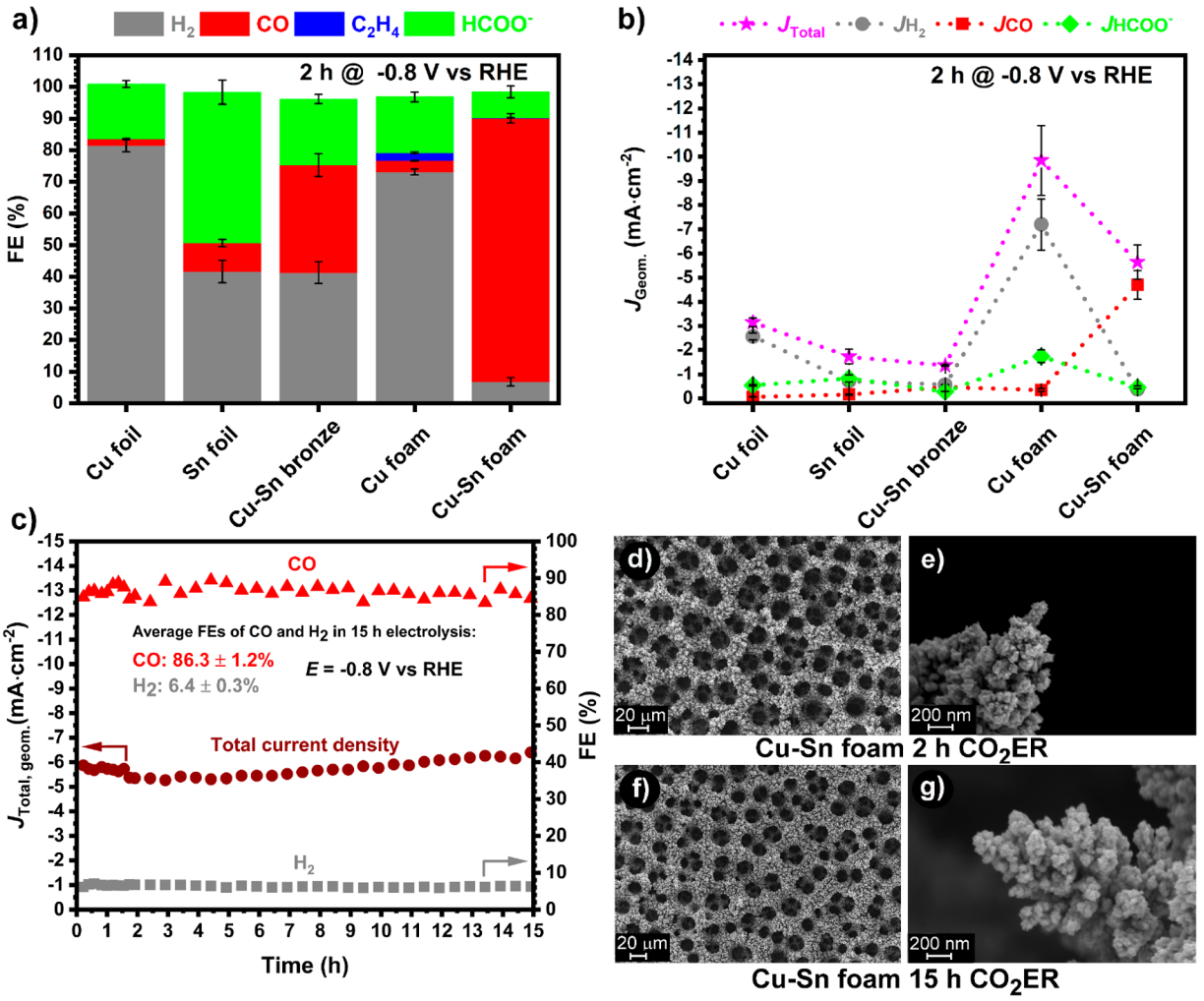

Figure 3. Selectivity and activity comparison at −0.8 V vs RHE: (a) distribution of FEs and (b) partial current densities. (c) Cu−Sn foam 15 h electrocatalytic durability test at −0.8 V vs RHE. SEM images of (d, e) Cu−Sn foam after 2 h and (f, g) after 15 h electrolysis. The FE and *J* results are expressed as average values ± average mean absolute error.

be attributed to its higher electrochemically active surface area together with its appropriate Cu−Sn surface composition (discussed below) compared to the bare Cu−Sn bronze (Figure S12 and Table S6). The best obtained electrocatalytic activity results for the Cu−Sn foam in terms of the FE and the partial current density for CO are quite comparable to the results reported for Sn-decorated Cu foams at identical applied potentials.[16,19]

On the other hand, the enhanced CO_2ER selectivity of the Cu−Sn foam toward CO compared to that of pure Cu foam cannot solely be attributed to the high electrochemically active surface area for both foams, even though the pure Cu foam has about half the surface roughness and gives ∼75% H_2 FE and only ∼5% CO at −0.8 V (Figure 3a). It is interesting to note that pure Cu foam with pore diameters between 50 and 100 μm was reported to convert CO_2 to C_2 products with 55% FE at the same applied potential in 0.5 mol·dm^{-3} $NaHCO_3$(aq) as a supporting electrolyte.[34] When that result is compared with those of the pure Cu foam demonstrated here (see Figure 3a and Table S5), it is obvious that the differences in the surface microstructure strongly affect the selectivity. However, in the case of the Cu−Sn foam, the presence of Sn surface sites plays an essential role in the CO_2 to CO selectivity enhancement accompanied by a significant decrease of the undesired HER. As mentioned above, the XPS analysis showed a slight variation between the surface compositions of the bare Cu−Sn bronze ($Cu_{14}Sn$) and the Cu−Sn foam ($Cu_{10}Sn$) (see Table S3), revealing that the electrodeposited foam has a higher Sn surface content than the starting material, for possible reasons discussed in section S1.4. Moreover, the Cu $2p_{3/2}$ peak position associated with Cu^0/Cu^+ oxidation states of the Cu−Sn foam is ∼1.0 eV negatively shifted (Figure S6a) compared to that observed on the Cu foil, pure Cu foam, and Cu−Sn bronze. Concurrently, the position of the Sn $3d_{5/2}$ peak associated with Sn^{2+} of the Cu−Sn foam is slightly shifted toward higher (0.2−0.3 eV) binding energy values (Figure S6c), in comparison with the peak positions in the Cu−Sn bronze and Sn foil spectra. This might suggest a difference in the charge redistribution between Cu and Sn in the Cu−Sn foam versus the Cu−Sn bronze arising from the changing of the Cu/Sn surface ratio.[20] This could be another contributor to the observed enhanced CO_2ER on the Cu−Sn foam.

The deconvolution of the surface roughness from the composition effect is aided by comparing the electrocatalytic activity of the Cu−Sn bronze with the activity to foils of Cu and Sn because all materials exhibit a near-planar surface

https://doi.org/10.1021/acsami.1c05015
ACS Appl. Mater. Interfaces 2021, 13, 38161−38169

(Figure 3a,b). The Cu−Sn bronze supports ∼7- and 3-fold higher J_{CO} compared to that of the Cu and Sn foils, respectively. Besides, it shows ∼4.5-fold lower J for H_2 than the Cu foil, whereas Sn foil gives ∼3- and 1.5-fold higher J for $HCOO^-$ compared to that of the Cu−Sn bronze and Cu foil, respectively (Figure 3b). Therefore, as expected, the activity variations on the Cu−Sn bronze when compared to that of its constituent elements can be attributed to intrinsic electrocatalytic activity properties of the bimetallic Cu−Sn system compared to those of pure Cu and Sn, which are further discussed below.

Nevertheless, as mentioned above, comparing the surface roughness effect on the activity of the Cu−Sn foam versus the pure Cu foam is not straightforward because the pure Cu foam showed about half the electrochemically active surface area (see Table S6) of the Cu−Sn foam but gave about 2 times the total current density and 10 times less J_{CO} together with far lower FE for CO than the Cu−Sn foam, as seen in Figure 3a,b. Thus, the significantly enhanced CO selectivity on Cu−Sn foam cannot simply be attributed to its higher electrochemically active surface area—rather the Cu−Sn surface composition is believed to be the key parameter. This claim is supported by the electrocatalytic activity results obtained on two control Cu−Sn foam samples with higher surface Sn content. The first control sample was prepared from a Sn-saturated electrodeposition solution, which refers to the electrodeposition solution that was repeatedly used to achieve the optimal CO_2 to CO performance of the Cu−Sn foam electrocatalyst (more details can be found in section S1.4). The Cu−Sn foam that was prepared from this electrodeposition solution has a Cu/Sn surface ratio of 1.4, a much higher Sn surface amount than $Cu_{10}Sn$ foam prepared from the optimal electrodeposition solution (Tables S3 and S4). A second control sample was prepared as a Sn-rich foam with $Cu_{0.6}Sn$ surface composition (see Figure S15). These foams with surface compositions of $Cu_{1.4}Sn$ and $Cu_{0.6}Sn$ showed ∼1.3 and 2 times lower J_{CO}, respectively, with an increase of the FEs for the HER and $HCOO^-$ at −0.8 V within a decrease of the Cu/Sn surface ratio (see Figure S15), despite their comparable electrochemically active surface area. Indeed, the selectivity of Cu−Sn foam shifts from CO to $HCOO^-$ with the increase of the Sn surface sites. This is an intrinsic property of the Cu−Sn CO_2ER electrocatalysts, where their selectivity can be tuned toward either CO or $HCOO^-$ via tuning the Cu/Sn surface ratio. This switching of the selectivity is generally attributed to the mutual perturbation of Cu and Sn electronic structures, which alters the preferential adsorption modes of the key intermediates.[20,35−37] Cu-rich Cu−Sn materials are found to drive the selectivity toward CO through stabilizing the C-bound adsorption mode of the *COOH key intermediate, whereas the O-bound *OCHO* pathway dominates on Sn-rich surfaces and thus favors the CO_2ER to $HCOO^-$,[20,36] as presented in Scheme S1. Besides affecting the absorption modes of the CO_2-derived intermediates, Sn weakens the adsorption of the *H intermediate, thus suppressing the HER.[11,35−37]

The durability of the Cu−Sn foam ($Cu_{10}Sn$ surface composition, Table S3) was examined at −0.8 V for 15 h. It maintained high activity for CO production with a FE > 85% and a partial current density of over −5 $mA{\cdot}cm^{-2}$ for (cf. Figure 3c and Figure 2c,d) retaining the dendrite morphology (Figure 3d−g and Figures S16 and S18) and the Cu/Sn = 10 surface composition (Table S3) during continuous electrolysis, indicating its stability. Indeed, the robustness and high CO selectivity of the Cu−Sn foam with dendrite microstructures prepared via one-pot, scalable, and fast DHBT is signifying that the utilization of the waste Cu−Sn bronze using this approach is a viable approach. Furthermore, according to previous reports, electrocatalysts with interconnected channels[38] and dendrite microstructures can promote CO_2 mass transport and thus prevent local CO_2 depletion near the electrode surface.[16,19,29]

Similarly, as in the case of the as-prepared Cu−Sn foam, the EDX mapping results after 2 and 15 h of CO_2 continuous electrolysis, data displayed in Figures S17 and S19, show good distribution of Cu and Sn over the entire foam, and again the EDX quantification showed much lower bulk abundance of the Sn in comparison with that of the pristine Cu−Sn bronze (Table S3). This suggests that the DHBT coelectrodeposition mechanism favors faster deposition of Cu over Sn in the bulk of the material, thus distributing the Sn on the surface of the dendrite microstructures as observed from the XPS results (Table S3). This is expected because Cu has a much lower exchange current and thus requires a lower overpotential for the formation of hydrogen templated foam morphology in comparison with Sn, which shows rather poor HER activity,[31,39] and pure Sn foam cannot be electrodeposited under the DHBT conditions we used in this study (see section S1.4).

When novel electrocatalyst materials are being studied, the avoidance of impurities such as trace metals is certainly important for obtaining a precise understanding of the intrinsic activity.[40−42] But production of high-purity materials is costly and resource-intensive, presenting challenges to upscaling. As mentioned above, the transition to sustainable energy systems will require massive amounts of raw materials with limited supply, so the utilization of recycled or repurposed materials is favored over increasing the rates of extraction from the Earth.[6] With this study, we showed that industrial-grade waste material that contains detectable impurities (see Table S1) can be used as raw material for fabrication of efficient and selective electrocatalysts. In fact, when comparing to the best published Cu−Sn-based catalysts optimized for CO selectivity and produced under careful synthetic conditions,[11−13,16,19] we find that our catalyst exhibited comparable or better CO selectivity, CO partial current density, and stability (compared at −0.8 V, for materials tested in CO_2-saturated aqueous solutions Table S7). This result shows promise that efficient catalysts can be produced from impure common materials such as industrial wastes. Although a proper techno-economic analysis would be needed to directly compare the repurposing of waste Cu−Sn bronze for electrocatalyst preparation against the conventional recycling methods (based on remelting), it is already apparent that repurposing a bulk material into a high surface area heterogeneous catalyst can be accomplished with efficient and minimized utilization of the starting material and without requiring high-temperature processes, as compared to bulk processing methods. Furthermore, the catalyst synthesis approach yields a product with a more specialized technological value and can contribute to the urgent goals of mitigating fossil carbon extraction and greenhouse gas emissions, as compared to the energy- and resource-intensive bulk recycling processes.

https://doi.org/10.1021/acsami.1c05015
ACS Appl. Mater. Interfaces 2021, 13, 38161−38169

CONCLUSIONS

In conclusion, we demonstrate a method for preparation of a CO-selective CO_2 conversion electrocatalyst via utilization of waste industrial Cu−Sn bronze. The approach identifies a straightforward and attractive route for repurposing waste material composed of Cu and Sn, metals which are on the list of elements with future endangered supply. The method is simple, fast, and controllable and requires no high-purity or expensive precursors, high temperatures, or sophisticated equipment. By a simple one-step DHBT coelectrodeposition method, Cu and Sn are transferred from a Cu−Sn bronze anode onto a surface of a cathode as a composite with a foam morphology that consists of dendrite microstructures and $Cu_{10}Sn$ surface stoichiometry. The as-prepared Cu−Sn foam has a slightly different Cu/Sn surface ratio and much higher surface roughness compared to the pristine Cu−Sn bronze, which results in a significant increase of the selectivity toward CO (FE > 85%) simultaneously with a great suppression of the thermodynamically favored H_2 evolution reaction (FE ∼ 5%) at a moderate applied potential of −0.8 V versus RHE in an aqueous electrolyte. The total C1-CO_2ER products' FE can reach values that are higher than 95%. The dendrite microstructures showed remarkable stability during 15 h of continuous electrolysis, thus preserving the electrocatalytic activity and Cu−Sn surface composition. Finally, the DHBT method serves as a proof-of-concept that such waste materials can be repurposed for electrocatalytic applications, with potential to be further developed and optimized for preparation of electrocatalysts on alternative substrates, such as gas diffusion electrodes, which can be implemented in larger scale CO_2 electrolyzers.[18]

ASSOCIATED CONTENT

Supporting Information

The Supporting Information is available free of charge at https://pubs.acs.org/doi/10.1021/acsami.1c05015.

Specifications of the utilized chemicals, materials, and techniques; synthesis procedures for creating Cu−Sn foams using the dynamic hydrogen bubble templated electrodeposition technique; data and methods for determination of electrochemically active surface area, Tafel slopes, and faradaic efficiencies of products; additional figures for characterization of the synthesized materials' morphology and composition including SEM images, elemental mapping, XPS, and XRD; cross-sectional SEM analysis of the synthesized Cu and Cu−Sn foams; additional electrochemical characterization data; table comparing the performance reported herein with other published results on similar materials (PDF)

AUTHOR INFORMATION

Corresponding Authors

Matthew T. Mayer − *Helmholtz Young Investigator Group: Electrochemical Conversion of CO_2, Helmholtz-Zentrum Berlin für Materialen und Energie GmbH, Berlin D-14109, Germany;* orcid.org/0000-0001-5379-2775; Email: m.mayer@helmholtz-berlin.de

Gumaa A. El-Nagar − *Helmholtz Young Investigator Group: Electrochemical Conversion of CO_2, Helmholtz-Zentrum Berlin für Materialen und Energie GmbH, Berlin D-14109, Germany;* orcid.org/0000-0001-8209-4597; Email: gumaa.el-nagar@helmholtz-berlin.de

Authors

Sasho Stojkovikj − *Helmholtz Young Investigator Group: Electrochemical Conversion of CO_2, Helmholtz-Zentrum Berlin für Materialen und Energie GmbH, Berlin D-14109, Germany; Institut für Chemie und Biochemie, Freie Universität Berlin, Berlin D-14195, Germany;* orcid.org/0000-0002-3346-2143

Frederik Firschke − *Helmholtz Young Investigator Group: Electrochemical Conversion of CO_2, Helmholtz-Zentrum Berlin für Materialen und Energie GmbH, Berlin D-14109, Germany; Institut für Chemie und Biochemie, Freie Universität Berlin, Berlin D-14195, Germany*

Laura C. Pardo Pérez − *Helmholtz Young Investigator Group: Electrochemical Conversion of CO_2, Helmholtz-Zentrum Berlin für Materialen und Energie GmbH, Berlin D-14109, Germany*

Léo Choubrac − *Department Structure and Dynamics of Energy Materials, Helmholtz-Zentrum Berlin für Materialen und Energie GmbH, Berlin D-14109, Germany;* orcid.org/0000-0003-3236-6376

Metodija Najdoski − *Institute of Chemistry, Faculty of Natural Sciences and Mathematics, Ss. Cyril and Methodius University Skopje, Skopje 1000, Republic of North Macedonia*

Complete contact information is available at: https://pubs.acs.org/10.1021/acsami.1c05015

Notes

The authors declare no competing financial interest.

ACKNOWLEDGMENTS

We thank the industrial smelting facility RŽ Institut AD Skopje, N. Macedonia, for donating the Cu−Sn bronze ingots that were used in this research. The authors acknowledge Veronica Davies, Alexander Arndt, Ursula Michalczik, Christian Höhn, Holger Kropf, and Siddharth Gupta for experimental support. This work was funded by the Helmholtz Association's Initiative and Networking Fund via the Helmholtz Young Investigators Group award (VH-NG-1225) and the Helmholtz-Climate-Initiative (HI-CAM). Instrumentation provided by the Helmholtz Energy Materials Foundry (HEMF) laboratories was used in this study.

ABBREVIATIONS USED

CO_2ER, electrochemical reduction of CO_2
DHBT, dynamic hydrogen bubbling template
EDX, energy dispersive X-ray spectrometry
FE, faradaic efficiency
GI-XRD, grazing-incidence X-ray diffraction
HER, hydrogen evolution reaction
ICP-OES, inductively coupled plasma-optical emission spectrometry
PTFE, polytetrafluoroethylene
SEM, scanning electron microscopy
XPS, X-ray photoelectron spectroscopy
XRF, X-ray fluorescence spectrometry

REFERENCES

(1) Chen, W.-Y.; Suzuki, T.; Lackner, M. *Handbook of Climate Change Mitigation and Adaptation*; Springer International Publishing: 2017. DOI: 10.1007/978-3-319-14409-2.

(2) De Luna, P.; Hahn, C.; Higgins, D.; Jaffer, S. A.; Jaramillo, T. F.; Sargent, E. H. What Would it Take for Renewably Powered

Electrosynthesis to Displace Petrochemical Processes? *Science* **2019**, *364* (6438), eaav3506.
(3) Kortlever, R.; Shen, J.; Schouten, K. J. P.; Calle-Vallejo, F.; Koper, M. T. M. Catalysts and Reaction Pathways for the Electrochemical Reduction of Carbon Dioxide. *J. Phys. Chem. Lett.* **2015**, *6* (20), 4073−4082.
(4) Jouny, M.; Luc, W.; Jiao, F. General Techno-Economic Analysis of CO_2 Electrolysis Systems. *Ind. Eng. Chem. Res.* **2018**, *57* (6), 2165−2177.
(5) de Klerk, A. Fischer−Tropsch Process. *Kirk-Othmer Encyclopedia of Chemical Technology* **2013**, 1−20.
(6) Sovacool, B. K.; Ali, S. H.; Bazilian, M.; Radley, B.; Nemery, B.; Okatz, J.; Mulvaney, D. Sustainable Minerals and Metals for a Low-Carbon Future. *Science* **2020**, *367* (6473), 30−33.
(7) Haas, T.; Krause, R.; Weber, R.; Demler, M.; Schmid, G. Technical Photosynthesis Involving CO_2 Electrolysis and Fermentation. *Nat. Catal.* **2018**, *1* (1), 32−39.
(8) Wu, J.; Huang, Y.; Ye, W.; Li, Y. CO_2 Reduction: From the Electrochemical to Photochemical Approach. *Adv. Sci.* **2017**, *4* (11), 1700194.
(9) Lee, S.; Choi, M.; Lee, J. Looking Back and Looking Ahead in Electrochemical Reduction of CO_2. *Chem. Rec.* **2020**, *20* (2), 89−101.
(10) Burkart, M. D.; Hazari, N.; Tway, C. L.; Zeitler, E. L. Opportunities and Challenges for Catalysis in Carbon Dioxide Utilization. *ACS Catal.* **2019**, *9* (9), 7937−7956.
(11) Sarfraz, S.; Garcia-Esparza, A. T.; Jedidi, A.; Cavallo, L.; Takanabe, K. Cu−Sn Bimetallic Catalyst for Selective Aqueous Electroreduction of CO_2 to CO. *ACS Catal.* **2016**, *6* (5), 2842−2851.
(12) Zhao, Y.; Wang, C.; Wallace, G. G. Tin Nanoparticles Decorated Copper Oxide Nanowires for Selective Electrochemical Reduction of Aqueous CO_2 to CO. *J. Mater. Chem. A* **2016**, *4* (27), 10710−10718.
(13) Li, Q.; Fu, J.; Zhu, W.; Chen, Z.; Shen, B.; Wu, L.; Xi, Z.; Wang, T.; Lu, G.; Zhu, J.-j.; Sun, S. Tuning Sn-Catalysis for Electrochemical Reduction of CO_2 to CO via the Core/Shell Cu/SnO_2 Structure. *J. Am. Chem. Soc.* **2017**, *139* (12), 4290−4293.
(14) Schreier, M.; Héroguel, F.; Steier, L.; Ahmad, S.; Luterbacher, J. S.; Mayer, M. T.; Luo, J.; Grätzel, M. Solar Conversion of CO_2 to CO using Earth-Abundant Electrocatalysts Prepared by Atomic Layer Modification of CuO. *Nat. Energy* **2017**, *2* (7), 17087.
(15) Hu, H.; Wang, Y.; Du, N.; Sun, Y.; Tang, Y.; Hu, Q.; Wan, P.; Dai, L.; Fisher, A. C.; Yang, X. J. Thermal-Treatment-Induced Cu−Sn Core/Shell Nanowire Array Catalysts for Highly Efficient CO_2 Electroreduction. *ChemElectroChem* **2018**, *5* (24), 3854−3858.
(16) Zeng, J.; Bejtka, K.; Ju, W.; Castellino, M.; Chiodoni, A.; Sacco, A.; Farkhondehfal, M. A.; Hernández, S.; Rentsch, D.; Battaglia, C.; Pirri, C. F. Advanced Cu-Sn Foam for Selectively Converting CO_2 to CO in Aqueous Solution. *Appl. Catal., B* **2018**, *236*, 475−482.
(17) Vasileff, A.; Xu, C.; Ge, L.; Zheng, Y.; Qiao, S.-Z. Bronze Alloys with Tin Surface Sites for Selective Electrochemical Reduction of CO_2. *Chem. Commun.* **2018**, *54* (99), 13965−13968.
(18) Ju, W.; Jiang, F.; Ma, H.; Pan, Z.; Zhao, Y.-B.; Pagani, F.; Rentsch, D.; Wang, J.; Battaglia, C. Electrocatalytic Reduction of Gaseous CO_2 to CO on Sn/Cu-Nanofiber-Based Gas Diffusion Electrodes. *Adv. Energy Mater.* **2019**, *9* (32), 1901514.
(19) Ju, W.; Zeng, J.; Bejtka, K.; Ma, H.; Rentsch, D.; Castellino, M.; Sacco, A.; Pirri, C. F.; Battaglia, C. Sn-Decorated Cu for Selective Electrochemical CO_2 to CO Conversion: Precision Architecture beyond Composition Design. *ACS Appl. Energy Mater.* **2019**, *2* (1), 867−872.
(20) Vasileff, A.; Zhi, X.; Xu, C.; Ge, L.; Jiao, Y.; Zheng, Y.; Qiao, S.-Z. Selectivity Control for Electrochemical CO_2 Reduction by Charge Redistribution on the Surface of Copper Alloys. *ACS Catal.* **2019**, *9* (10), 9411−9417.
(21) Zhang, S.-N.; Li, M.; Hua, B.; Duan, N.; Ding, S.; Bergens, S.; Shankar, K.; Luo, J.-L. A Rational Design of Cu_2O−SnO_2 Core-Shell Catalyst for Highly Selective CO_2-to-CO Conversion. *ChemCatChem* **2019**, *11* (16), 4147−4153.
(22) Zhao, S.; Li, S.; Guo, T.; Zhang, S.; Wang, J.; Wu, Y.; Chen, Y. Advances in Sn-Based Catalysts for Electrochemical CO_2 Reduction. *Nano-Micro Lett.* **2019**, *11* (1), 62.
(23) Yoo, C. J.; Dong, W. J.; Park, J. Y.; Lim, J. W.; Kim, S.; Choi, K. S.; Odongo Ngome, F. O.; Choi, S.-Y.; Lee, J.-L. Compositional and Geometrical Effects of Bimetallic Cu−Sn Catalysts on Selective Electrochemical CO_2 Reduction to CO. *ACS Appl. Energy Mater.* **2020**, *3* (5), 4466−4473.
(24) Poliakoff, M.; Licence, P.; George, M. W. UN Sustainable Development Goals: How Can Sustainable/Green Chemistry Contribute? By Doing Things Differently. *Curr. Opin. Green Sustain. Chem.* **2018**, *13*, 146−149.
(25) Endangered Elements. https://www.acs.org/content/acs/en/greenchemistry/research-innovation/endangered-elements.html (accessed 2021-05-12).
(26) Radu, S.; Demian, M.; Demian, G.; Ciobanu, M. Studies on the Possibility of Recycling Waste Bronze. *Adv. Mater. Res.* **2015**, *1128*, 303−311.
(27) Gálvez-Vázquez, M. d. J.; Moreno-García, P.; Guo, H.; Hou, Y.; Dutta, A.; Waldvogel, S. R.; Broekmann, P. Leaded Bronze Alloy as a Catalyst for the Electroreduction of CO_2. *ChemElectroChem* **2019**, *6* (8), 2324−2330.
(28) Greenblatt, J. B.; Miller, D. J.; Ager, J. W.; Houle, F. A.; Sharp, I. D. The Technical and Energetic Challenges of Separating (Photo)Electrochemical Carbon Dioxide Reduction Products. *Joule* **2018**, *2* (3), 381−420.
(29) Burdyny, T.; Graham, P. J.; Pang, Y.; Dinh, C.-T.; Liu, M.; Sargent, E. H.; Sinton, D. Nanomorphology-Enhanced Gas-Evolution Intensifies CO_2 Reduction Electrochemistry. *ACS Sustainable Chem. Eng.* **2017**, *5* (5), 4031−4040.
(30) Hui, S.; Shaigan, N.; Neburchilov, V.; Zhang, L.; Malek, K.; Eikerling, M.; Luna, P. D. Three-Dimensional Cathodes for Electrochemical Reduction of CO_2: From Macro- to Nano-Engineering. *Nanomaterials* **2020**, *10* (9), 1884.
(31) Vesztergom, S.; Dutta, A.; Rahaman, M.; Kiran, K.; Zelocualtecatl Montiel, I.; Broekmann, P. Hydrogen Bubble Templated Metal Foams as Efficient Catalysts of CO_2 Electroreduction. *ChemCatChem* **2021**, *13* (4), 1039−1058.
(32) Hall, A. S.; Yoon, Y.; Wuttig, A.; Surendranath, Y. Mesostructure-Induced Selectivity in CO_2 Reduction Catalysis. *J. Am. Chem. Soc.* **2015**, *137* (47), 14834−14837.
(33) Yoon, Y.; Hall, A. S.; Surendranath, Y. Tuning of Silver Catalyst Mesostructure Promotes Selective Carbon Dioxide Conversion into Fuels. *Angew. Chem., Int. Ed.* **2016**, *55* (49), 15282−15286.
(34) Dutta, A.; Rahaman, M.; Luedi, N. C.; Mohos, M.; Broekmann, P. Morphology Matters: Tuning the Product Distribution of CO_2 Electroreduction on Oxide-Derived Cu Foam Catalysts. *ACS Catal.* **2016**, *6* (6), 3804−3814.
(35) He, J.; Dettelbach, K. E.; Huang, A.; Berlinguette, C. P. Brass and Bronze as Effective CO_2 Reduction Electrocatalysts. *Angew. Chem., Int. Ed.* **2017**, *56* (52), 16579−16582.
(36) Vasileff, A.; Xu, C.; Jiao, Y.; Zheng, Y.; Qiao, S.-Z. Surface and Interface Engineering in Copper-Based Bimetallic Materials for Selective CO_2 Electroreduction. *Chem.* **2018**, *4* (8), 1809−1831.
(37) Wu, Y.; Iwase, K.; Harada, T.; Nakanishi, S.; Kamiya, K. Sn Atoms on Cu Nanoparticles for Suppressing Competitive H_2 Evolution in CO_2 Electrolysis. *ACS Appl. Nano Mater.* **2021**, *4*, 4994.
(38) Hyun, G.; Song, J. T.; Ahn, C.; Ham, Y.; Cho, D.; Oh, J.; Jeon, S. Hierarchically Porous Au Nanostructures with Interconnected Channels for Efficient Mass Transport in Electrocatalytic CO_2 Reduction. *Proc. Natl. Acad. Sci. U. S. A.* **2020**, *117* (11), 5680−5685.
(39) Nikolić, N. D. Influence of the Exchange Current Density and Overpotential for Hydrogen Evolution Reaction on the Shape of Electrolytically Produced Disperse Forms. *J. Electrochem. Sci. Eng.* **2020**, *10* (2), 111−126.
(40) Lum, Y.; Kwon, Y.; Lobaccaro, P.; Chen, L.; Clark, E. L.; Bell, A. T.; Ager, J. W. Trace Levels of Copper in Carbon Materials Show Significant Electrochemical CO_2 Reduction Activity. *ACS Catal.* **2016**, *6* (1), 202−209.

https://doi.org/10.1021/acsami.1c05015
ACS Appl. Mater. Interfaces 2021, 13, 38161−38169

(41) Wuttig, A.; Surendranath, Y. Impurity Ion Complexation Enhances Carbon Dioxide Reduction Catalysis. *ACS Catal.* **2015**, *5* (7), 4479−4484.
(42) Pander, J. E., III; Ren, D.; Yeo, B. S. Practices for the Collection and Reporting of Electrocatalytic Performance and Mechanistic Information for the CO_2 Reduction Reaction. *Catal. Sci. Technol.* **2017**, *7* (24), 5820−5832.

https://doi.org/10.1021/acsami.1c05015
ACS Appl. Mater. Interfaces 2021, 13, 38161−38169